Available online at www.sciencedirect.com

ScienceDirect

Procedia CIRP 110 (2022) 273–278

www.elsevier.com/locate/procedia

V CIRP Conference on Biomanufacturing

3D Printing and Computational Modeling for the Evaluation of LVOT obstruction in Transcatheter Mitral Valve Replacement

Chiara Catalano[a], Stefano Cannata[b], Valentina Agnese[b],

Gianluca Buffa[a], Livan Fratini[a], Salvatore Pasta[a]*, Caterina Gandolfo[b]

[a]*Department of Engineering, University of Palermo, Viale delle Scienze Ed. 8, Palermo 90128, Italy*
[b]*Department for the Treatment and Study of Cardiothoracic Transplantation, IRCCS-ISMETT, via Tricomi 5, 90128, Palermo, Italy*

* Corresponding author. Tel.: +39 334 9379694. *E-mail address:* salvatore.pasta@unipa.it

Abstract

Transcatheter mitral valve replacement (TMVR) is an emerging alternative treatment for those patients not qualified for surgery. However, TMVR can determine an obstruction of the left ventricular outflow tract (namely, neo-LVOT) induced by the transcatheter heart valve (THV) displacing the native mitral valve leaflet towards the myocardial wall. This condition can lead to haemodynamic impairment and ultimately patient death. We sought to predict the neo-LVOT obstruction by first developing patient-specific simulations of the THV deployment and then comparing predictions with post-TMVR diagnostic images and 3D printed human models. Using pre-TMVR computed-tomography (CT) imaging, patient-specific anatomies of two patients were reconstructed and then meshed with ABAQUS/Explicit solver. The latter was used to simulate the crimping and deployment of SAPIEN 3 THV (Edwards Lifesciences, Irvine, CA) and then simulate the cardiac beating. The neo-LVOT cross sectional area was then computed. For both patients, rigid heart models were printed with SLS rapid prototyping technology while the SAPIEN 3 device was printed with flexible resin to manually positioning the device in the human host.
Numerical predictions and 3D printed model measurements of neo-LVOT area agreed well with those obtained by post-TMVR CT imaging. Both computational modelling and 3D printing revealed a comprehensive assessment of the TMVR feasibility, which is not readily conferred by conventional CT imaging. Particularly, the realistic printed models could become an efficient and indispensable tool to help the heart team visualizing the LVOT obstruction to anatomical scale, in a life-size replica of patient-specific cardiac anatomy.

Keywords: 3D priting; finite-element simulation; transcatheter heart valve

1. Introduction

Transcatheter mitral valve replacement (TMVR) is an alternative percutaneous treatment for those patients not eligible for mitral valve surgery. There is however an unmet need in the development of devices designed for TMVR because of the complex mitral valve anatomy and its sub-apparatus structure. Thus, TMVR relies upon the off-label use of transcatheter heart valves (THV) specifically designed for the aortic valve replacement [1].

The off-label application of balloon expandable THVs implanted in mitral position for inoperable patients, i.e., in the case of degenerated bio-prostheses (valve in valve), failed annuloplasty (valve in ring) or calcified annulus (valve in MAC) is gaining widespread acceptance thanks to encouraging clinical evidence and the new-generation of THVs reducing the risk of adverse complications [2-4]. Accomplishing TMVR in valve-in-MAC (i.e., Mitral Annular Calcification) can be even more challenging due to i) the possible absence of a circumferential annular calcification and a stable anchoring

10.1016/j.procir.2022.06.049

zone, and ii) the quite stiff calcification portending to annulus rupture during THV deployment.

TMVR provides many challenges referring to occurrence of feared complications, i.e., left ventricular outflow tract (LVOT) obstruction. The implantation of the percutaneous device in the mitral position leads to a permanent displacement of the anterior mitral valve leaflet towards the interventricular septum, thus resulting in an elongation of the outflow tract into the left ventricle. The newly generated elongation is known as neo-LVOT and is a major concern in TMVR [1, 5]. Recently, the initial report of the first multicenter global registry for TMVR has suggested the occurrence of LVOT obstruction with hemodynamic compromise in the 8.2% patients population with valve-in-ring and valve-in-bioprosthesis, with rates increasing upon 9.3% in the setting of valve-in-MAC [6].

Imaging is the gold-standard to assess the feasibility of TMVR for a given patient. According to clinical recommendations, a neo-LVOT area < 170 mm^2 as measured by CT imaging after TMVR denotes a high risk of adverse events and death. To provide a pre-procedural planning of TMVR, computational simulations and 3D printing could provide new insights on the feasibility and efficacy of TMVR as well as the assessment of the neo-LVOT area in patients with valve-in-MAC [1, 2].

This study aims to quantify the biomechanical consequences of the neo-LVOT in two patients affected by mitral annular calcification (MAC) using both numerical simulations and 3D printed human heart models. The proposed computational workflow combines CT scans to reconstruct patient-specific anatomies that were used for both finite-element analyses and 3D printing to test the efficacy of pre-TMVR procedure. We simulated the crimping and deployment of the SAPIEN 3 (S3) THV (Edwards Lifesciences, Irvine, CA) and compared neo-LVOT predictions between simulations end 3D printed human models.

2. Methods

2.1. TMVR Procedure

We investigated the case of two patients (A and B) affected by mitral annular calcification underwent transapical TMVR procedure at ISMETT IRCCS hospital. According to the clinical considerations and the amount of calcification, the percutaneous approach was declared suitable by the Heart Team due to the elevated surgical risk of patients. For both patients, the optimal size of the S3 THV was assessed on the basis of pre-operative CT imaging measurements and patients' medical history. The THV size was identified by measuring the annulus diameter from pre-operative CT data. Specifically, the balloon expandable S3 Ultra (Edwards Lifesciences, USA) with dimensions of 26 mm was selected for both patients. TMVR was accomplished in a cardiac catheterization lab or hybrid operating room with the patient under anesthesia. Transoesophageal echocardiography (TEE) and fluoroscopic guidance assist the deployment of the S3 Ultra device, which occurred after balloon inflation and rapid pacing (150 – 200 bpm).

2.2. Finite Element Analysis

The computational analysis consisted of a finite element simulation of the S3 Ultra THV deployment in a patient-specific heart model. We assessed the amount of the anterior mitral valve leaflet displacement, the Mises stress exerted on device frame and the resulting neo-LVOT area.

2.3. Heart Domain

The heart structure was reconstructed by segmenting electrogram (ECG) – gated computed tomography scans *via* image dedicated segmentation techniques implemented in Mimics (Materialise, Leuven, Belgium) [7-10]. 3D segmentation of the left atrium, left ventricle, mitral annular calcification and aorta was carried out at end-diastolic phase by applying multiple masks at various specific grey intensity values (Hounsfield units, HU). This was done by means of semiautomatic thresholding followed by manual masks editing. Smoothing and wrapping algorithms were adopted to soften the geometry and obtain a fine mesh quality still maintaining native heart anatomy unaltered. Smoothing was applied with Laplace filter factor of 0.25 and 25 iterations, while wrapping algorithm was characterized by 0.8 mm of smallest detail and 1.5 mm of gap closing distance. Resulting masks were then thickened in Rhino CAD software (v.5.5, McNeel & associates, SP) [5]. The output of segmented file was a .stl file to be used for the human model manufacturing by 3D printing.

2.4. THV Model

The S3 Ultra THV represents a balloon expandable, radiopaque, cobalt – chromium frame with trileaflet bovine pericardial tissue valve and a sealing skirt made of polyethylene terephthalate (PET) [5, 11]. The CAD model of S3 Ultra of 26 mm was obtained by the acquisition of the S3 Ultra device using a high-resolution micro-CT scanner (Skyscan 1272, Bruker, USA).

Table 1 summarizes the meshing parameters of each anatomic part obtained using the software ICEM (v.21, Ansys, USA). Specifically, the metallic frame was discretized with structured hexahedral solid elements with reduced integration (C3D8R). The stress-free configuration of the outer sealing skirt was modelled at mid-thickness of the crimped stent by closing cell geometries using several surfaces. These surfaces had size of 0.1 mm and were meshed with triangular shell elements (S3R). The inner skirt and the expandable balloon were discretized as surfaces with triangular membrane elements (M3D3). The delivery system here adopted relies upon the Edwards Novaflex delivery system, which is composed of an expandable balloon generated in Rhino by revolution of the balloon shape profile around the centerline [5].

Table 1. Meshing parameters.

Part Name	Mesh Size (mm)	Element Type	Element number (thousands)
Patient A			
Left Ventricle	4 – 2	Tetrahedral	77.8 – 77.9
Left Atrium	3 – 2	Tetrahedral	26.7
Ascending Aorta	2 – 1	Tetrahedral	19.5 – 19.7
Calcification	2	Tetrahedral	30.7
MV Leaflets	1	Triangular	1.8 – 1.9
Patient B			
Left Ventricle	4 – 2	Tetrahedral	70.6 – 70.7
Left Atrium	3 – 2	Tetrahedral	26.8
Ascending Aorta	2 – 1	Tetrahedral	28.8 – 28.9
Calcification	2	Tetrahedral	13
MV Leaflets	1	Triangular	1.7

2.5. Material properties

The left atrium, mitral valve, calcification and aorta were modelled as linear elastic isotropic material with density of D = 1060 kg/m^3, Poisson coefficient of $\nu = 0.45$ to account quasi-incompressible response and Young moduli of E = 1 MPa and E = 10 MPa, for the left atrium and calcification respectively. Regardless of the simplicity of these assumptions, the introduction of a different mechanical behaviour for the left atrium and aorta has demonstrated an overall realistic response. In a different way, both passive response and active tissue contraction characterize the left ventricular mechanical behaviour. Thus, we used the Holpzapfel and Ogden anisotropic hyperelastic formulation to model the passive material response, while the active behaviour was achieved by additional stress in the fiber direction. This was accomplished by a time dependent elastance model based on the formulation of Walker and collaborators [12, 13]. Local cylindric coordinate systems (θ=40°) were used to define the cardiac fiber network of the myocardium.

The S3 Ultra cobalt-chromium alloy frame was described by Von Mises plasticity and isotropic hardening while the PET skirt was modelled by an elasto-plastic response [14, 15]. The balloon behaviour was portrayed as linear elastic material with density of D = 1060 kg/m^3. Table 2 summarizes the adopted material parameters for each anatomic parts and device of the numerical simulation.

Table 2. Material properties; E=Young Modulus, ν=Poisson Coefficient, σ_y=Yield Stress, σ_{ult}= Ultimate Tensile Stress, ε_p=Plastic Strain, D=Density.

	E (MPa)	ν	σ_y (MPa)	σ_{ult} (MPa)	ε_p	D (kg/m^3)
Heart Parts	1	0.45				1060
Calcification	10	0.45				1060
S3 Stent	233x10^3	0.35	414	930	0.45	8000
Sealing Skirt	55	0.49	6.6	6.6	0.6	8000
Balloon	600	0.3				1060

2.6. TMVR Simulation

The Abaqus/Explicit finite element solver (v.2020 Dassault Systèmes, Paris, France) was used for numerical simulations, allowing to consider a dynamic non-linear problem in the range of large deformation and complex contact interactions [16]. Cardiac beating was firstly performed without device for both patient A and B, then the crimping of the device and its subsequently deployment and balloon-based expansion were replicated. The general Abaqus contact algorithm was used to account for the interaction among anatomic parts and the device. Tie contacts were imposed between the mitral valve and the calcifications, between the aorta and ventricle and between the atrium and calcifications. Rigid constraints were applied to the left atrium and aorta in the longitudinal direction as boundary conditions. A mass scaling of 1.0e-6 was used to reduce the computational cost. Specifically, a quasi-static solution was provided by ensuring that the ratio of kinetic to internal energy was <10% [5, 17]. The cardiac beat was 0.7 sec long and started with the diastolic filling.

S3 Ultra crimping was achieved by progressively reducing the size of a rigid dodecahedral surface from the initial diameter (i.e., 26 mm) to the final diameter of 4.5 mm. The surface was discretized with 1500 structured-quadrilateral elements with reduced integration and density is D = 7000 kg/m^3. Contact conditions were generated between the S3 device and the balloon during the deployment. Tie contact conditions were used between the sealing skirt surface and the S3 Ultra frame.

The balloon geometry reported by Bailey and collaborators was used in this study [18]. The deflated balloon configuration was achieved using a surface as described for the crimping of S3 Ultra frame. The deflated balloon was then integrated with the crimped valve, and then this assembly was properly aligned into the mitral annulus. The balloon expansion to the nominal diameter of S3 Ultra was simulated using the fluid-cavity approach implemented in Abaqus [5].

2.7. 3D Printed Models

3D printing was focused on the geometry of the left ventricle. The left atrium and aorta were not included to achieve an open geometry, thereby allowing a direct visualization of S3-related obstruction. Prior to 3D printing, the segmented masks were edited to delete the left ventricular apex and support the device implantation from the inner heart side. Anatomical models were exported from the medical imaging software as. stl format and then printed by SLS rapid prototyping technology (Sinterit, 3DiTALY) in grey nylon powder (PA12). A layer thickness of 0.1 mm was used to capture the changes in the curvature of the heart models.

We also printed the frame of S3 Ultra device, and this resulted in a relatively flexible model given the thin design frame of the device (0.1 mm). For the rigid patient-specific heart models, we were able to manually implant the 3D printed THVs model in the mitral valve position, according to manufacturer guidelines.

Specifically, the THV device was placed coaxially with

respect to mitral valve annulus and with 1/3 of the device height anchored to left atrium and the remaining portion inside the left ventricle [19]. To measure the neo-LVOT area, we first photographed the printed models with a ruler and then quantified the obstruction in imaging software.

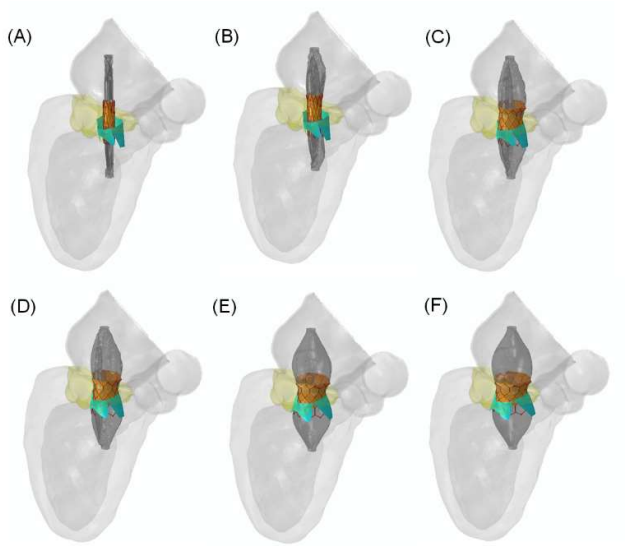

Fig. 1. Different steps of THV deployment by balloon expansion.

3. Results

Fig. 1 shows the THV deployment with expansion occurring using a balloon filling of 21 mL. We can observe the progress of the deployment and anchoring of S3 Ultra THV to the calcified annulus in correspondence of the first and second cell stent rows (images A to C), and the MV leaflets permanent displacement due to stent frame (images D to F).

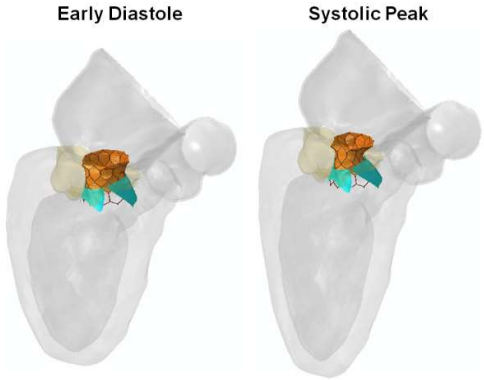

Fig. 2. Early diastolic and peak systolic configuration of Patient A heart.

Fig. 2 provides the actual configuration of Patient A at two cardiac phases: the early diastole and systolic peak. Patient B had anatomic constraints that limited the THV implantation and reduced remarkably the native LVOT anatomy. Both anterior leaflets revealed to be shifted toward the interventricular septum, resulting in high grade of displacement with respect to the posterior ones.

Fig. 3 shows the Von Mises stress distribution exerted on the THV frame.

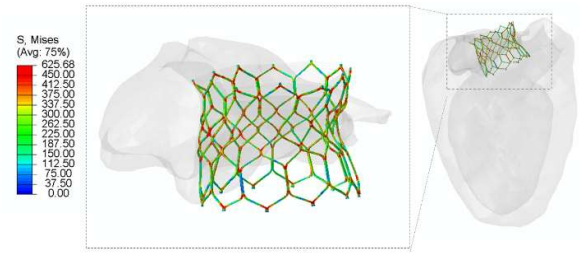

Fig. 3. Von Mises stress distribution (MPa) of S3 metallic frame at end of diastole.

Neo-LVOT area was calculated using a workflow suggested by Blanke and collaborators [20]. This consisted of first generating a geometric centerline along the axis of the ascending aorta and LVOT and then calculating the cross-sectional area at the level of the smallest neo-LVOT area formed by the virtually implanted THV and the septum [20, 21]. We found that Patient A had a neo-LVOT area of 372.5 mm^2 while Patient B had neo-LVOT area of 46.3 mm^2 as shown by Fig. 4.

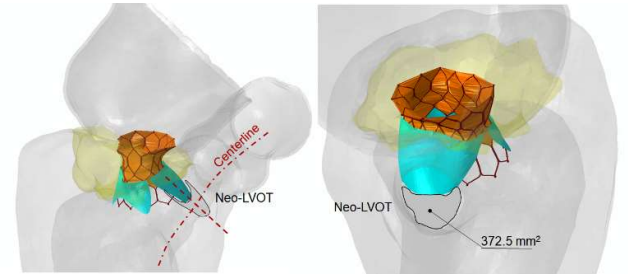

Fig. 4. LVOT obstruction and estimation of neo-LVOT area for Patient A.

The printed left ventricles with the manually implanted THVs have been used for quantifying the obstruction and then for comparison with computational findings. Prototypes have favored an adequate visualization and assessment of LVOT obstruction as illustrated by Fig. 5. We also found a good agreement between the computational models and the 3D printed anatomy, e.g. prediction of 372.5 mm^2 versus 3D printed neo-LVOT area of 327. 9 mm^2 for Patient A, and prediction of 46.3 mm^2 versus 3D printed neo-LVOT area of 55.7 mm^2 for Patient B. 3D printing confirmed that Patient A could be a candidate for TMVR while Patient B is not suitable because of the lack of adequate space in the left ventricle, likely portending hemodynamic impairment.

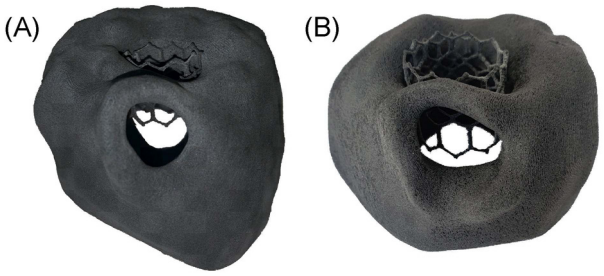

Fig. 5. 3D printed models for (A) Patient A and (B) Patient B showing the obstruction of neo-LVOT as seen from the aortic lumen.

4. Discussion

Given the complex and dynamic nature of mitral valve apparatus and the clinical burdens associated to TMVR, the blend of patient-specific simulations and 3D printing has demonstrated a potential for pre-operative planning of TMVR and for guiding prophylactic intervention.

This study provided new insights in the biomechanics of TMVR when devices are implanted off-labels to treat patients with severe MAC, and assess the performance of implanted device, i.e., the quantification of the neo-LVOT area. Patient A had a neo-LVOT area quite above the clinical cut-off value of 170 mm^2, making the TMVR a feasible option in this individual. Backwards, Patient B had a neo-LVOT area that is quite below the clinical cut-off, thus suggesting a patient anatomy not eligible for the percutaneous treatment.

The threat of left ventricular outflow tract obstruction in valve-in-ring, valve-in-valve and valve-in-MAC patients has been recently recognized as a fatal complication in the setting of TMVR. The length of the anterior mitral leaflet, the mitral-aortic angle, the thickness of the interventricular septum, the size of LVOT and the left ventricle cavity strongly are considered key anatomic factors portending adverse outcome [2, 22]. Valve size and implantation depth also influence the outcome of TMVR as the risk of LVOT obstruction increases as THV diameter and implantation depth increase [1]. Using a combination of computational modeling and 3D printing, we envision a new paradigm of predictive and personalized medicine in which the interventional cardiologist can plan the optimal device position and size in a human model to reduce the risk of adverse events prior to TMVR procedure.

Notwithstanding, structural mechanics of the heart and outcomes prediction after TMVR by means of computational and printed models is poorly explored. Few studies simulated TMVR through personalized computational analysis and 3D printing and highlighted the impact of device morphology and patient anatomy and the hemodynamic implications after the procedure [21, 23]. Recently, we provided an overall assessment of LVOT obstruction implications in valve-in-ring TMVR by accomplishing computational structural and fluid dynamical analyses, demonstrating the value of computational modeling predictions against post-TMVR CT imaging [5].

The here presented numerical simulation allowed to mimic the S3 Ultra crimping and deployment and the beating action of the heart, leading to the estimation of the Mises stress resulting from the interaction of the human host with the device. As calcifications represent the landing zone for the THV frame, thus preventing any possible malpositioning or displacement of the device, a careful pre-TMVR planning is demanding to avoid THV failure especially for borderline anatomy as that of Patient B. It could be suggested that the balloon expansion might have the potential to induce annulus rupture with an incidence that could increase with the stiffness, the amount and morphology of MAC as well as the oversizing of the THV device. Since a comprehensive analysis of mitral annular calcification material properties does not exist yet, these considerations should be confirmed in future studies.

The relevant stiffness of the calcified annulus implies the generation of important anchoring forces on the metallic frame, which arise and overpass, at specific nodes the value of yield stress and could lead to significant asymmetric mechanical deformations or stent damage. Specifically, Patient A experienced the highest value of Mises stress in the metallic frame at the level of the anterior MV leaflet, while Patient B stress values are more significant and appear to be alarmingly greater than the ultimate stress of the THV stent, ultimately leading to device failure and patient death.

Clearly, the amount of both dynamical and morphological risk factors, and the complexity in the elliptical landing zone require a careful pre-procedural imaging, which commonly involves echocardiographic evaluation along with multiphase cardiac CT. However, these techniques provide standard geometric measurements, which likely might be lacking in predicting adverse events related to TMVR. Conventional imaging cannot effectively predict potential procedure pitfalls because of the incapacity (i) to select the most suitable THV to the mitral annulus affected by significant calcification, (ii) to guess how calcification will response to radial stress and (iii) to predict the relationship between possible risk factors and insurgence of LVOT obstruction [24]. In this perspective, computational modeling and 3D printed models may be the key for improving the management of patients undergoing TMVR.

3D prototyping allowed our group to accurately replicate the patient-specific heart and valve models into physical ones, which are crucial for preprocedural planning, patient education and physician direct interpretation of the case, without requiring any special training in imaging. Furthermore, these phantoms allowed to simulate the anticipated procedural anatomic alterations, i.e., anterior leaflet resection or alcohol septal ablation, and eventually elucidate their contribute to the TMVR.

Of course, this study presents several limitations that need to be undertaken, and additional validation is required to confirm the added value of our numerical and experimental findings. In this context, a step forward should be the development of a more realistic computational workflow, which accounts the compliance ranged from the relationship between the filling of blood and the contraction. The 3D printed models should be manufactured using flexible materials to reproduce the heart compliance instead of rigid models as here proposed.

5. Conclusion

Our patient-specific numerical modelling and physical manufacturing of human hearts highlighted the complex mechanism behind TMVR procedure and the potential to predict adverse events as the LVOT obstruction. Validation will be performed by comparison with CT imaging and clinical information. We conclude that computer simulation and 3D printing may refine the conventional imaging, by improving patient stratification and outcomes after TMVR in the setting of mitral annular calcification.

Acknowledgements

This study was supported by a grant from Edwards Lifescience (THV-I20-532- Sim4Sapien) to SP.

References

1. Ferrari, E., D. Dvir, and M. Guerrero, *Transcatheter mitral valve replacement in degenerated calcified native mitral valves: is the currently available technology suitable?* 2016, Oxford University Press. p. 391-395.
2. Yoon, S.-H., et al., *Predictors of left ventricular outflow tract obstruction after transcatheter mitral valve replacement.* JACC: Cardiovascular Interventions, 2019. **12**(2): p. 182-193.
3. Yoon, S.-H., et al., *Transcatheter mitral valve replacement for degenerated bioprosthetic valves and failed annuloplasty rings.* Journal of the American College of Cardiology, 2017. **70**(9): p. 1121-1131.
4. Muller, D.W., et al., *Transcatheter mitral valve replacement for patients with symptomatic mitral regurgitation: a global feasibility trial.* Journal of the American College of Cardiology, 2017. **69**(4): p. 381-391.
5. Pasta, S., et al., *Simulation of left ventricular outflow tract (LVOT) obstruction in transcatheter mitral valve-in-ring replacement.* Medical Engineering & Physics, 2020. **82**: p. 40-48.
6. Guerrero, M., et al., *Transcatheter mitral valve replacement in native mitral valve disease with severe mitral annular calcification: results from the first multicenter global registry.* JACC: Cardiovascular Interventions, 2016. **9**(13): p. 1361-1371.
7. Fratini, L., G. Macaluso, and S. Pasta, *Residual stresses and FCP prediction in FSW through a continuous FE model.* Journal of Materials Processing Technology, 2009. **209**(15-16): p. 5465-5474.
8. Fratini, L. and S. Pasta, *Residual stresses in friction stir welded parts of complex geometry.* International Journal of Advanced Manufacturing Technology, 2012. **59**(5-8): p. 547-557.
9. Pasta, S., et al., *Three-dimensional parametric modeling of bicuspid aortopathy and comparison with computational flow predictions.* Artif Organs, 2017. **41**(9): p. E92-E102.
10. Comelli, A., et al., *Deep learning approach for the segmentation of aneurysmal ascending aorta.* Biomedical Engineering Letters, 2021. **11**(1): p. 15-24.
11. Pasta, S., et al., *Simulation study of transcatheter heart valve implantation in patients with stenotic bicuspid aortic valve.* Med Biol Eng Comput, 2020. **58**(4): p. 815-829.
12. Walker, J.C., et al., *MRI-based finite-element analysis of left ventricular aneurysm.* American Journal of Physiology-Heart and Circulatory Physiology, 2005. **289**(2): p. H692-H700.
13. Gao, H., et al., *Parameter estimation in a Holzapfel–Ogden law for healthy myocardium.* Journal of engineering mathematics, 2015. **95**(1): p. 231-248.
14. Mao, W., et al., *Fully-coupled fluid-structure interaction simulation of the aortic and mitral valves in a realistic 3D left ventricle model.* PloS one, 2017. **12**(9): p. e0184729.
15. Morganti, S., et al., *Simulation of transcatheter aortic valve implantation through patient-specific finite element analysis: two clinical cases.* Journal of biomechanics, 2014. **47**(11): p. 2547-2555.
16. Pasta, S., et al., *Transcatheter Heart Valve Implantation in Bicuspid Patients with Self-Expanding Device.* Bioengineering-Basel, 2021. **8**(7).
17. Baillargeon, B., et al., *The living heart project: a robust and integrative simulator for human heart function.* European Journal of Mechanics-A/Solids, 2014. **48**: p. 38-47.
18. Bailey, J., N. Curzen, and N.W. Bressloff, *Assessing the impact of including leaflets in the simulation of TAVI deployment into a patient-specific aortic root.* Computer methods in biomechanics and biomedical engineering, 2016. **19**(7): p. 733-744.
19. Blanke, P., et al., *Mitral annular evaluation with CT in the context of transcatheter mitral valve replacement.* JACC: Cardiovascular Imaging, 2015. **8**(5): p. 612-615.
20. Blanke, P., et al., *Predicting LVOT obstruction in transcatheter mitral valve implantation: concept of the neo-LVOT.* JACC: Cardiovascular Imaging, 2017. **10**(4): p. 482-485.
21. Kohli, K., et al., *Transcatheter mitral valve planning and the Neo-LVOT: utilization of virtual simulation models and 3D printing.* Current treatment options in cardiovascular medicine, 2018. **20**(12): p. 1-14.
22. Maisano, F. and M. Taramasso, *Mitral valve-in-valve, valve-in-ring, and valve-in-MAC: the Good, the Bad, and the Ugly.* European heart journal, 2019.
23. El Sabbagh, A., et al., *Three‐dimensional prototyping for procedural simulation of transcatheter mitral valve replacement in patients with mitral annular calcification.* Catheterization and Cardiovascular Interventions, 2018. **92**(7): p. E537-E549.
24. Karády, J., et al., *Transcatheter mitral valve replacement in mitral annulus calcification–"The art of computer simulation".* Journal of cardiovascular computed tomography, 2018. **12**(2): p. 153-157.